JNeurosci
THE JOURNAL OF NEUROSCIENCE

Research Articles: Behavioral/Cognitive

Temporal expectation modulates the cortical dynamics of short-term memory

Anna Wilsch[1,2], Molly J. Henry[1,3], Björn Herrmann[1,3], Christoph S. Herrmann[2] and Jonas Obleser[1,4]

[1]*Max Planck Research Group "Auditory Cognition", Max Planck Institute for Human Cognitive and Brain Sciences, Leipzig, Germany*

[2]*Experimental Psychology Lab, Center for Excellence "Hearing4all," European Medical School, University of Oldenburg, Oldenburg, Germany*

[3]*Department of Psychology, Brain and Mind Institute, University of Western Ontario, London, Ontario, Canada*

[4]*Department of Psychology, University of Lübeck, Lübeck, Germany*

DOI: 10.1523/JNEUROSCI.2928-17.2018

Received: 11 October 2017

Revised: 9 July 2018

Accepted: 10 July 2018

Published: 16 July 2018

Author contributions: A.W., M.J.H., B.H., and J.O. designed research; A.W., M.J.H., B.H., and J.O. performed research; A.W. analyzed data; A.W., M.J.H., B.H., C.S.H., and J.O. wrote the paper.

Conflict of Interest: The authors declare no competing financial interests.

Research was supported by a Max Planck Research Group grant (J.O.). The authors declare no competing financial interests. The authors are grateful to Burkhard Maess and Yvonne Wolff-Rosier for help with MEG data acquisition. Three anonymous reviewers helped improve the manuscript with their constructive comments.

Corresponding authors: Anna Wilsch, Email: anna.wilsch@gmail.com, Jonas Obleser, Department of Psychology, Universität zu Lübeck, MFC 8, Maria-Goeppert-Straße 9a, 23562 Lübeck, Germany, Email: jonas.obleser@uni-luebeck.de

Cite as: J. Neurosci ; 10.1523/JNEUROSCI.2928-17.2018

Temporal expectation modulates the cortical dynamics of short-term memory

Anna Wilsch[1,2], Molly J. Henry[1,3], Björn Herrmann[1,3], Christoph S. Herrmann[2], & Jonas Obleser[1,4]

[1]Max Planck Research Group "Auditory Cognition", Max Planck Institute for Human Cognitive and Brain Sciences, Leipzig, Germany
[2]Experimental Psychology Lab, Center for Excellence "Hearing4all," European Medical School, University of Oldenburg, Oldenburg, Germany
[3]Department of Psychology, Brain and Mind Institute, University of Western Ontario, London, Ontario, Canada
[4]Department of Psychology, University of Lübeck, Lübeck, Germany

Running title: Cortical dynamics in short-term memory

Corresponding authors:
Anna Wilsch
Email: anna.wilsch@gmail.com

Jonas Obleser
Department of Psychology
Universität zu Lübeck
MFC 8, Maria-Goeppert-Straße 9a
23562 Lübeck, Germany
Email: jonas.obleser@uni-luebeck.de

Number of pages:	28
Number of figures:	5
Number of tables:	0
Number of multimedia and 3D models:	0

Number of words

Abstract:	237
Introduction:	712
Discussion:	1728

Acknowledgements:
Research was supported by a Max Planck Research Group grant (J.O.). The authors declare no competing financial interests. The authors are grateful to Burkhard Maess and Yvonne Wolff-Rosier for help with MEG data acquisition. Three anonymous reviewers helped improve the manuscript with their constructive comments.

Abstract

Increased memory load is often signified by enhanced neural oscillatory power in the alpha range (8–13 Hz), taken to reflect inhibition of task-irrelevant brain regions. The corresponding neural correlates of memory decay, however, are not yet well-understood. In the current study, we investigated auditory short-term memory decay in humans (male and female) using a delayed matching-to-sample task with pure-tone sequences. First, in a behavioral experiment we modeled memory performance over six different delay-phase durations. Second, in a magnetoencephalography (MEG) experiment, we assessed alpha-power modulations over three different delay-phase durations. In both experiments, the temporal expectation for the to-be-remembered sound was manipulated, so that it was either temporally expected or not. In both studies, memory performance declined over time but this decline was weaker when the onset time of the to-be-remembered sound was expected. Similarly, patterns of alpha power in and alpha-tuned connectivity between sensory cortices changed parametrically with delay duration (i.e., decrease in occipito-parietal regions, increase in temporal regions). Notably, temporal expectation not only counteracted alpha-power decline in heteromodal brain areas (i.e., supramarginal gyrus), but also had a beneficial effect on memory decay counteracting memory-performance decline. Correspondingly, temporal expectation also boosted alpha connectivity within attention networks known to play an active role during memory maintenance. The present data show how patterns of alpha power orchestrate short-term memory decay, and encourage a more nuanced perspective on alpha power across brain space and time beyond its inhibitory role.

Significance Statement

Our sensory memories of the physical world fade quickly. We show here that this decay of short-term memory can be counteracted by so-called temporal expectation, that is, knowledge of when to expect a sensory event that an individual must remember. We also show that neural oscillations in the “alpha” (8–13 Hz) range index both the degree of memory decay (for brief sound patterns) and the respective memory benefit from temporal expectation. Spatially distributed cortical patterns of alpha power show opposing effects in auditory vs. visual sensory cortices. Moreover, alpha-tuned connectivity changes within supramodal attention networks reflect the allocation of neural resources as short-term memory representations fade.

Introduction

Short-term memory allows us to focus our attention on representations of perceptions that are no longer physically present (Baddeley, 2012). This ability is limited, though, by memory load and memory decay. The amount and the precision of information in memory draw on capacity and must not exceed a certain limit (e.g., Luck and Vogel, 1997; van den Berg et al., 2012; Ma et al., 2014; Joseph et al., 2016). Neural oscillations in the alpha range (8–13 Hz), recorded using human electroencephalography (EEG) or magnetoencephalography (MEG), are modulated by manipulations of memory load. For example, alpha power increases as the number of items held in memory increases (Jensen et al., 2002; Busch and Herrmann, 2003; Leiberg et al., 2006; Obleser et al., 2012). This alpha-power increase is thought to protect the storage of items in memory (Roux and Uhlhaas, 2014) by functionally inhibiting task-irrelevant information and/or brain regions (Klimesch et al., 2007). However, it is less clear how neural oscillatory activity is related to memory decay.

Memory decay refers to fading away of the memory representation over time (Brown, 1958; Posner and Keele, 1967). Previous work on neural correlates of memory decay suggests a reduction of neural responses during the "delay phase", that is, the time during which information is held in memory before it can be reported or compared to another stimulus. Over the course of memory delay, single-cell activity in monkey prefrontal cortex decreases (Fuster, 1999), as does the BOLD response measured in posterior (Jha and McCarthy, 2000; for visual memory) and temporal (Gaab et al., 2003; for auditory memory) cortical regions in humans.

It is less clear to predict how alpha power should behave over the course of a memory delay phase. Given the relationship between BOLD responses and cortical alpha power (Sadaghiani et al., 2010), alpha power might well decrease. However, if we assume that alpha oscillations inhibit interference with memory representations, alpha power should increase over time, as more interference is to be expected. What is more, the expected direction of alpha change with fading short-term memory should depend on the brain area under consideration: An auditory area in temporal cortex, where short-term memory traces need protection (e.g., Strauß et al., 2014), and a visual area, where interference needs to be inhibited (Jensen and Mazaheri, 2010) might well show differential response patterns.

One factor that has the potential to counteract memory decay is temporal expectation. Detection and discrimination are more accurate for temporally expected compared to unexpected stimuli (Coull and Nobre, 1998; Griffin et al., 2001; Nobre, 2001; Jaramillo and Zador, 2011), and temporally expected events promote perceptual evidence accumulation (Cravo et al., 2013). Also, temporal expectation for a to-be-remembered stimulus reduces memory load for speech-in-noise, as indexed by improved memory performance (Wilsch et al., 2015). Notably, this load reduction co-occurred with decreased alpha power during stimulus maintenance, suggestive of temporal expectation effects persisting into the delay phase. Moreover, temporally expected distractors are more easily kept out of short-term memory. This effect is also accompanied by increased alpha power in anticipation of an

expected distractor (Bonnefond and Jensen, 2012). It is unclear, however, whether temporal expectation also has a beneficial effect on memory decay (see Kunert and Jongman, 2017).

Here we report the results of two experiments investigating the time course of decay in short-term memory (Cowan, 1984; Cowan et al., 1997; Nees, 2016). Auditory short-term memory enables integration of auditory information and preservation of information over brief periods of time (Schröger, 2007). We conducted a delayed pitch comparison procedure (e.g., Harris, 1952; Bachem, 1954; Bull and Cuddy, 1972; Keller et al., 1995) with two brief pure-tone sequences embedded in noise, separated by variable delay phases, asking whether the sequences were the same as or different from each other.

Experiment 1 probed and modelled memory performance over six increasing delay phases addressing the question whether temporal expectation affects memory decay behaviorally. Experiment 2 investigated the interaction of temporal expectation and memory decay at the neural level. The focus was on neural alpha (~8–13 Hz) oscillatory dynamics during the maintenance of the expected (or not expected) stimulus as a remote effect of temporal expectation on memory decay. Alpha power modulations were assessed on the sensor level as well as by means of source analyses and functional connectivity.

Methods

Participants

In Experiment 1 (behavior and modelling), $N = 19$ healthy right-handed participants (12 females; age range 23–33 years, median 25 years) took part. In Experiment 2 (behavior and MEG recordings), an independent sample of $N = 20$ healthy right-handed participants (10 females; age range 23–33 years, median 27 years) took part. All participants had self-reported normal hearing. The local ethics committee (University of Leipzig) approved of the studies in accordance with the Declaration of Helsinki. Participants were fully debriefed about the nature and goals of the studies, and provided written informed consent prior to testing. All participants received financial compensation of 7 € per hour for their participation.

Experimental task and stimuli

The time course of an example trial is depicted in Figure 1A. On each trial, participants heard two pure-tone sequences (S1 and S2, see "Characteristics of sound stimuli") and responded whether they were the same or different. These pure-tone sequences were embedded in noise, in order to increase perceptual load (Pichora-Fuller and Singh, 2006; van den Berg et al., 2012). We made use of non-verbal stimuli to preclude rehearsal effects (Obleser and Eisner, 2009; Oberauer and Lewandowsky, 2013) and thus to keep any effects interpretable in terms of short-term memory.

Each trial began with the presentation of a fixation cross. After a brief pause (jittered between 0.75 s and 1.25 s), white noise and a visual cue were presented simultaneously. The visual cue indicated the

onset time of the first sound (S1; see next paragraph) and remained on screen throughout the entire trial. Participants had to retain S1 in memory for a variable period of time. Then, a second sound (S2) was presented, and participants made a "same"/"different" judgment by pressing one of two buttons on a response box. The response was prompted approximately 1 second (jittered between 0.9 s and 1.1 m) after the presentation of S2. Finally, participants indicated their confidence in their "same"/"different" response on a 3-level confidence scale ("not at all confident", "somewhat confident", "very confident"). Trials were separated by an inter-trial interval of around 1 second (jittered: 0.75–1.25 s) that was free of stimulation or responses. See Figure 1A for an outline of a trial.

Operationalization of memory decay and temporal expectation

Memory decay was manipulated by varying the time interval (delay phase) between S1 and S2. The aim of Experiment 1 was to fit an exponential decay function to memory performance across different delay-phase durations. To this end, the delay-phase duration was varied logarithmically in six steps ranging between 0.6 and 7 s (i.e., 0.6, 1, 1.6, 2.6, 4.3, 7 s; see Figure 1B, left panel). In Experiment 2, delay phases were more coarsely sampled (1, 2, and 4 seconds; see Figure 1D, left panel).

Temporal expectation for S1 was manipulated by varying the S1-onset times relative to the presentation of a visual cue. Onset times were either fixed (i.e., S1 occurred 1.3 s after the onset of the visual cue) or jittered (i.e., S1 occurred after a duration drawn from a uniform distribution ranging between .9 s and 1.7 s, mean = 1.3 s.

Characteristics of the sound stimuli

All sound stimuli were sequences consisting of five pure tones; each pure tone had a duration of 40 ms resulting in a total sound duration of 200 ms (Watson et al., 1975). Sound stimuli were presented in standard–deviant pairs. For the standard stimulus, the middle (third) tone's frequency was randomly selected on each trial from a uniform distribution ranging between 450 and 600 Hz. The second and fourth tones were independently assigned frequencies ±1–4 semitones (ST) with respect to the frequency of the middle tone, and the first and final tones were independently assigned frequencies ±4–7 ST with respect to the middle tone. Unique patterns were generated on each trial.

On half of the trials, a deviant stimulus was presented (i.e., "different" trials). For the deviant stimulus, the third and the fourth pure tone in the sequence were higher in frequency compared to S1. The third and fourth tones were both shifted up by the same amount (in ST; see Procedure). The exact standard-to-deviant-difference was adjusted for each participant individually (see "Procedure"). Each pure tone had an onset- and offset-ramp of 10 ms. On half of the trials, the standard stimulus was presented during the S1 interval, while the deviant stimulus was presented during the S1 interval the other half of the trials.

The noise masker was white noise. Sound sequences and noise were presented with a constant signal-to-noise ratio (SNR) of –17 dB. This SNR was determined via pilot testing to increase difficulty of the memory task but still allow all participants to perform the task.

Procedure

Prior to the MEG measurement, participants were familiarized with the stimuli and task, and performed a few practice trials. Then, individual thresholds were estimated (i.e., the frequency difference between standard and deviant in the third and fourth pure tone position of the sound sequences). A custom adaptive-tracking procedure was utilized that yielded a frequency difference corresponding to memory performance falling between 65% and 85% correct responses.

In Experiment 1, participants completed 360 trials in 10 blocks of 36 trials each. In Experiment 2, brain activity was recorded with MEG during the performance of 396 trials completed in 12 blocks of 33 trials each. The manipulation of S1-onset time (fixed, jittered) was kept constant within a block, and participants were informed at the start of each block about the type of temporal cue they would receive on each trial. Delay-phase durations (0.6–7 seconds, and 1-, 2-, 4-seconds, for Experiment 1 and 2 respectively) were equally distributed within blocks. The order of trials within a block and order of blocks were randomized for each participant. Button assignments were counterbalanced across participants, such that half of the participants indicated that the first and the second sound were the same using the left button, and half did so with the right button.

The testing took approximately 2.5 hours per participant and was conducted within one session. The overall session including practice blocks and preparation of the MEG setup took about 4 hours.

Modelling of behavioral data in Experiment 1

Data analysis

The crucial measure for memory decay was the performance measure Az, a non-parametric performance measure derived from confidence ratings. Hit and false alarm rates at each confidence level were used to construct receiver operating characteristic (ROC) curves (Macmillan and Creelman, 2004) for each condition, and ROC curves were used to derive Az. Az corresponds to the area under the ROC curve and can be interpreted similarly to proportion correct. Az was computed for each of the twelve conditions (temporal expectation, 2, × memory decay, 6), allowing us to estimate memory decay as a function of delay-phase duration separately for fixed and jittered onset times. One participant had to be excluded from this analysis because the participant did not make use of the entire confidence rating scale in at least two experimental conditions; Az could not be computed for these data points. Another participant presented the same behavior but only in one condition. Here, the missing Az value was interpolated by calculating the mean of the two adjacent conditions.

We fitted Equation 1 (Glass and Mackey, 1988) to Az scores as a function of delay-phase duration:

$$x(t) = x_0 + e^{-\gamma t} + \frac{\lambda}{\gamma}(1 - e^{-\gamma t}) \quad (1)$$

where t is equal to time (i.e., delay-phase duration) and x_0 corresponds to the intercept. This specific function contained a term describing decay, γ, and an additional term describing growth, λ. The ratio $\frac{\lambda}{\gamma}$ indicates the function's asymptote.

Note that, compared to simple decay functions (e.g., Wickelgren, 1969; Rubin and Wenzel, 1996), this function bears the advantage that it takes the nature of physiological systems into account. That is, it assumes that in physiological systems activations decline while competing, new activations arise. This interaction of decay and growth applies to short-term memory in the following sense: The stored memory representation decays over time. According to so-called resource models of short-term memory, allocation of cognitive resources (i.e., growth of activation) can counteract this decay (for a review, see Ma et al., 2014). Short-term memory has been argued to operate by effectively focusing attention on the memory representation (e.g., Cowan 1999). This concept has been supported by findings of neural activity during the delay phase representing active storage mechanisms (e.g., Roux & Ulhaas, 2014). Furthermore, prefrontal cortex activity has also been reported to be involved in active maintenance processes (Bauer & Fuster 1976; Funahashi et al. 1993; for a review see D'Esposito, 2007).

The fit-initial parameters were as follows: $x_0 = 0$, $\gamma = 0$, and $\lambda = 0$, where x_0 was bound between zero and one, and γ and λ were bound between zero and infinity. The model fit was computed with the lsqcurvefit function with Matlab (version 8.2, Optimization Toolbox) that allowed for 1000 iterations.

In addition, we also fitted a decay-term–only model (i.e., first term: $x(t) = (x_0 + e^{-\gamma t})$). The decay-only model is more parsimonious and more commonly used to estimate memory decay (Peterson and Peterson, 1959; Wickelgren, 1969). To determine which one of these two models represented the memory performance data best, we calculated the Bayesian information criterion (BIC; Schwarz, 1978) for both model fits, as well as for fixed and jittered onset times separately. Note that the BIC penalizes for more parameters and allows for an equitable comparison of goodness-of-fit of both models (smaller is better). We averaged the BICs across fixed and jittered onset times separately for each function. 17 out of 18 participants had a lower BIC for the full model (Equation 1) than the decay-only model indicating an overall better fit by the former model. Therefore, all further analyses were conducted on the parameters resulting from the fit of the complete Equation 1. Four of the participants were excluded from subsequent analyses, because R^2, an indicator for goodness of the model fit, of their fitted models was smaller than 0.3 (see Figure 1C for individual model fits). The average R^2 values for the fixed and jittered conditions, respectively, were 0.66 (sd = 0.31; 0.80, sd = 0.13 without excluded participants) and 0.72 (sd = 0.25; 0.81, sd = 0.16 without excluded participants).

After the fitting of the function, the resulting parameters x_0, γ, and λ for jittered and fixed onset times as dependent variables were assessed with a multivariate ANOVA. This allowed us to test

whether there is a global difference between jittered and fixed onset times. Subsequently, the parameters γ, λ, and x_0 were tested for differences between fixed and jittered onset times with univariate repeated-measures ANOVAs, to determine whether memory decay was less strong when S1-onset times were predictable.

Data recording and analysis in Experiment 2

Participants were seated in an electromagnetically shielded room (Vacuumschmelze, Hanau, Germany). Magnetic fields were recorded using a 306-sensor Neuromag Vectorview MEG (Elekta, Helsinki, Finland) with 204 orthogonal planar gradiometers and 102 magnetometers at 102 locations. Two electrode pairs recorded a bipolar electrooculogram (EOG) for horizontal and vertical eye movements. The participants' head positions were monitored during the measurement by five head position indicator (HPI) coils. Signals were sampled at a rate of 1000 Hz with a bandwidth ranging from direct current (DC) to 330 Hz.

The signal space separation method was applied offline to suppress external interferences in the data, interpolate bad channels, and to transform individual data to a default head position that allows statistical analyses across participants in sensor space (Taulu et al., 2004).

Subsequent data analyses were carried out with Matlab (The MathWorks Inc., Massachusetts, USA) and the FieldTrip toolbox (Oostenveld et al., 2011) using only trials to which correct responses were provided ("correct trials"). Analyses were conducted using only the 204 gradiometer sensors, as they are most sensitive to magnetic fields originating directly underneath them (Hämäläinen et al., 1993). The continuous data were filtered offline with a 0.5-Hz high pass filter, specifically designed to provide a strong suppression of DC signals in the data (>140 dB at DC, 3493 points, Hamming window; e.g., Ruhnau et al., 2012).

Subsequently, trial epochs ranging from –1.5 to 11.5 s time-locked to the onset of S1 were defined. The use of long epochs prevented windowing artifacts in the time–frequency analysis; the intervals analyzed statistically were shorter (see below). Epochs were low-pass filtered at 80 Hz and subsequently down-sampled to 200 Hz.

Epochs with strong artifacts were rejected when the signal range at any gradiometer exceeded 800 pT/m. Independent component analysis (ICA) was applied to the epochs in order to reduce artifacts due to eye blinks and heartbeat. Following ICA, remaining epochs were rejected when the signal range within one epoch exceeded 200 pT/m (gradiometer) or 100 μV (EOG). Additionally, trials were rejected manually for which variance across sensors was deemed high relative to all others (per participant, per condition) based on visual inspection. For further analysis, each trial was time-locked at two different points, i.e., all trials were time-locked to the first stimulus (t = 0 s at S1 onset) and to the second stimulus (t = 0 s at S2 onset) for separate analyses. This was because different trials had different delay phase durations so that trials time-locked to S1 were not always time-locked to S2.

Spectral analysis

The analyses focus on responses time-locked to S2. This enabled us to examine the responses related to the end of the delay phase; the period during which we expected to find remote effects of temporal expectation for S1 on stimulus maintenance and thus on memory decay. For each trial, a 0.7-s segment was extracted (–0.8 to –0.1 s time-locked to S2 excluding evoked responses due to S1 sound presentation, see Figure 1A, light gray box), multiplied with a Hann taper, and the power between 8–13 Hz was computed using a fast Fourier transform (FFT).

For illustration purposes only, we also computed time–frequency representations (TFRs) of responses that were time-locked to S1. Time–frequency analysis was conducted on trial epochs ranging from –2.0 to 7.6 s for each trial (with 20-ms time resolution) for frequencies ranging between 0.5 Hz to 20 Hz (logarithmically spaced, in 20 bins). Single-trial time-domain data were convolved with a Hann taper, with an adaptive width of two to four cycles per frequency (i.e., 2 cycles for 0.5–1.6 Hz, 3 cycles for 1.9–9.2 Hz, and 4 cycles for 11.1–20 Hz). The output of the analysis was complex Fourier data. For further analyses, power (squared magnitude of the complex-valued TFR estimates) was averaged across single trials. Inter-trial phase coherence (ITPC) was computed based on the complex Fourier data (Lachaux et al., 1999). ITPC is the magnitude of the amplitude-normalized complex values averaged across trials for each time-frequency bin per channel and experimental condition (Thorne et al., 2011).

Next, FFT power spectra as well as TFRs were averaged across gradiometers in each pair. This procedure resulted in one single-trial value for each time point (TFRs only), frequency bin and sensor position for each delay-phase condition and onset-time condition.

Source localization

In order to estimate the origin of sensor-level alpha-power, source localizations were computed based on individual T1-weighted MRI images (3T Magnetom Trio, Siemens AG, Germany). Topographical representations of the cortical surface of each hemisphere were constructed with Freesurfer (http://surfer.nmr.mgh.harvard.edu) and the MR coordinate system was co-registered with the MEG coordinate system using the head-position indicators (HPIs) and about 100 additional digitized points on the head surface (Polhemus FASTRAK 3D digitizer). For forward and inverse calculations, boundary element models were computed for each participant using the inner skull surface as volume conductor (using the MNE toolbox; https://martinos.org/mne/). Individual mid-gray matter surfaces were used as source model by reducing the approximately 150,000 vertices needed to describe single hemispheres to 10,242 vertices.

The beamformer approach (DICS, dynamic imaging of coherent sources; Gross et al., 2001) was used to project alpha power (–0.8 to –0.1 s time-locked to S2-onset) to source space. To this end, a multitaper FFT centered at 11 Hz (±2 Hz smoothing with three Slepian tapers; Percival and Walden, 1993) was computed. A complex filter was calculated based on the data of all delay-phase and onset-

time conditions (Gross et al., 2001; Schoffelen et al., 2008). Single-trial complex FFT data were then projected through the filter, separately for each condition providing a power value for each frequency bin in the alpha range at each vertex.

Functional connectivity analyses

To attain a better understanding of the functional role of alpha power in memory decay, specifically for alpha power emerging from left superior temporal gyrus (STG, MNI [–50, –17, –8]), connectivity analyses between cortical sources were computed. Note that MNI coordinates were selected based on the source localization of the alpha power effect (see below). A whole-brain approach was adopted to find brain areas that were functionally connected with left STG on the basis of weighted pairwise phase consistency (wPPC; Vinck et al., 2010; see also Gulbinaite et al., 2017). The advantage of wPPC, over e.g., inter-trial phase coherence, is that wPPC is critically independent of the number of trials used in the calculation. Weighted PPC (wPPC) measures the consistency of phase angles between trial pairs. First, Fourier spectra from 8–13 Hz were calculated in the time window time-locked to S2 (–0.8 to –0.1 s) and multiplied by the previously calculated common DICS filter (see above). Then, we computed wPPC using the FieldTrip function ft_connectivity_ppc.m on the single-trial complex Fourier spectra. The greater the wPPC at a vertex the greater the phase consistency between this vertex and left STG.

Statistical analysis

Memory performance

Analogous to Experiment 1, memory performance for each condition was indexed by Az (see Figure 1D). To test whether there were differences in Az between experimental conditions (i.e., fixed and jittered onset times and delay phase duration), we computed a repeated measures ANOVA with both factors temporal expectation (fixed vs. jittered onset times) and memory decay (1-, 2-, 4-s delay-phase duration). In analogy to Experiment 1, we also assessed the difference in memory decay between fixed and jittered onset times. Since in Experiment 2 only three different delay-phase durations were employed instead of six, we were only able to compute a linear fit across these durations. Hence, memory decay was estimated by regressing Az on the delay phase durations of 1-, 2-, and 4 seconds. The impact of temporal expectation on memory decay was measured by comparing the slopes of the linear fit for fixed and jittered S1-onset times using a paired-samples t-test. Prior to all analyses, Az was linearized by computing a rationalized arcsine unit (RAU)-transformation (Studebaker, 1985). Furthermore, as effect size measures, we report partial η^2 for repeated-measures ANOVAs and $r_{equivalent}$ for dependent samples t-tests (Rosenthal and Rubin, 2003). Response times are not reported because responses were cue-prompted and thus would provide only partially valid information about costs and benefits of the experimental manipulations.

Sensor level analyses

Statistical analyses were conducted on the FFT power spectra (–0.8 to –0.1 time-locked to S2), according to a multi-level approach. On the first (single-subject) level, we regressed alpha power on the delay phase durations (1, 2, 4-s) similar to the regression of memory performance (Az) on delay phase duration (see above). To test the parametric modulation of memory decay, the FieldTrip-implemented independent-samples regression t-test was performed (Maris and Oostenveld, 2007). The regression t-test provides the regression b-coefficient (i.e., slope of the modulation) for each frequency bin at each of the 102 sensor positions indicating the strength of the tested contrast. Here, to test for a linear relationship between alpha power and delay phase duration, contrast coefficients were selected corresponding to the actual delay-phase duration in seconds (i.e., 1, 2, 4). To test whether temporal expectation had an impact on this relationship, the same contrast was calculated for fixed and jittered onset times separately.

For the statistical analyses on the second (group) level, b-values resulting from the first-level statistics testing the parametric modulations of alpha power by the delay phase were tested against zero. In addition, to test whether the delay-phase modulation in the fixed condition differs significantly from the modulation in the jittered condition, b-values attained for each of the onset-time conditions separately were tested against each other. The tests against zero as well as the tests contrasting fixed and jittered conditions were conducted with FieldTrip's dependent sample t-test using cluster-based permutation tests. The cluster test corrects for multiple comparisons resulting from testing each frequency-sensor combination. All cluster tests were two-tailed and were thus considered significant when $p < 0.025$.

We also tested for correlations between alpha power and memory performance (Az), averaging over experimental conditions, with a multi-level cluster test. On the first level, each participant's six RAU-transformed Az values (2 temporal-expectancy conditions × 3 delay phases) were correlated with the corresponding alpha-power values. On the second level, first-level correlation values were Fisher's z transformed and tested against zero with a dependent samples cluster-based permutation t-test.

Source level analyses

Statistical analyses for source-projected alpha power as well as for wPPC reflecting functional connectivity between left STG and any other vertex were conducted with the same approach. The aim was to test whether either variable (alpha power or wPPC) was modulated by delay-phase duration and whether this modulation was affected by temporal expectation.

Contrasts were calculated for each vertex separately. To test for a linear relationship of memory decay and alpha power in source space, source projected alpha power and the delay-phase duration (1, 2, 4 s) were z-transformed on a single-subject level. Then the delay phase duration served as a

regressor and was fitted to the source power to test for a linear relationship of alpha power and delay-phase duration. The same approach was applied to test for effects of functional connectivity: wPPCs were z-transformed and z-transformed delay-phase duration values were fitted to these wPPCs.

The resulting regression coefficients at each individual vertex from both contrasts were then spatially smoothed across the surface (vertices) using an approximation to a 6 mm FWHM Gaussian kernel (Han et al., 2006) and morphed onto a common surface in MNI space, respectively (Freesurfer average brain; Fischl et al., 1999b). For the interaction of temporal expectation and memory decay, the same linear regression was applied to the same data again but separately for each temporal-expectation condition. On the group level, regression coefficients of each contrast were tested against zero or fixed-onset-time coefficients were tested against jittered-onset-time coefficients, respectively, with vertex-wise t-tests. The resulting t-values were z-transformed and displayed on the average brain surface with contrast dependent uncorrected vertex-wise threshold of $|z| \geq 1.96$ (Sohoglu et al., 2012).

Then, brain regions that showed statistical effects were identified by extracting the MNI-coordinate of the greatest z-value within one area of interest. Areas of interest were identified by visual inspection. The MNI coordinate was then used to identify the specific brain region using the MNI structural atlas.

Correlation of alpha power and Az in source space

Analogous to the analyses on the sensor level, the correlation of source projected alpha power and Az was calculated by correlating RAU-transformed Az with alpha power within condition at each vertex point. Here as well, the Fisher's z-transformed correlation values were tested against zero with vertex-wise t-tests. The resulting t-values were z-transformed and displayed on the average brain surface with an uncorrected vertex-wise threshold of $|z| \geq 1.96$.

Results

In the present study, we investigated whether and how temporal expectation ameliorates the decay of sound representations in short-term memory. Participants retained a sound (S1) in memory for a delay phase that varied in duration from trial to trial and judged whether sound S1 was same or different from another sound (S2) presented after the delay phase. We focused on behavioral performance as well as on neural oscillatory activity in the alpha frequency band.

Experiment 1: Behavioral modelling of memory decay

In Experiment I, we estimated a "forgetting curve" based on fits of an exponential-decay function to Az values as a function of delay-phase duration. Fits were conducted separately for fixed and jittered S1-onset times to assess the effect of temporal expectation on memory decay. In line with the broad literature on short-term memory decay, Az declined with longer delay-phase durations. Interestingly, performance decayed differently for jittered and fixed onset times (Figure 1B). The two functions

(jittered and fixed) show that for delay-phases up to one second, memory performance was the same following fixed and jittered onset times, whereas for longer delay phases, performance declined less severely following fixed compared to jittered onset times. Figure 1C displays the single-subject fits of the decay function.

A multivariate ANOVA showed that the estimated parameters decay factor, growth factor, and intercept (Wilk's approximated $F(3,11) = 3.81$, $p = 0.043$, $\eta^2 = 0.51$) differed for fixed versus jittered S1-onset times. Subsequent univariate tests on all parameters separately revealed that there was a trend-level effect of the decay factor γ ($F(1,13) = 3.68$, $p = 0.077$, $\eta^2 = 0.221$; Figure 1B). The univariate test on the growth factor, λ, showed that growth over delay-phase duration was significantly greater for fixed than for jittered onset times ($F(1,13) = 4.95$, $p = 0.044$, $\eta^2 = 0.276$; Figure 1B), converging with the test on the decay factor (γ) that Az declines faster after jittered than after fixed onset times. The univariate test on the intercept x_0 did not show a difference between onset times ($F(1,13) = 0.04$, $p = 0.84$, $\eta^2 = 0.003$). Next, we tested both asymptotes separately against 0.5 (i.e., corresponding to memory performance at chance level). The asymptote parameter estimate corresponding to fixed onset times was significantly larger than chance as shown by a 95-% confidence interval (CI) of [0.52; 0.82], whereas the asymptote after jittered onset times did not differ from 0.5 [95% CI 0.26; 0.64] (Figure 1B). However, fixed and jittered asymptotes did not differ significantly from each other ($t(13) = 1.47$, $p = 0.164$, $r = 0.378$). Thus, while memory performance declines to chance level following jittered onset times for longer delays, fixed onset times counteract this decline in memory performance.

Experiment 2: Linear effects of memory decay and temporal expectation on behavioral performance

First, we computed a repeated-measures ANOVA on Az with the factors delay-phase duration and temporal expectation. The ANOVA on RAU-transformed Az yielded a significant main effect of delay-phase duration ($F(2,38) = 21.95$, $p < 0.0001$, $\eta^2 = 0.536$) but no main effect of temporal expectation ($F(1,19) = 3.20$, $p = 0.736$, $\eta^2 = 0.1441$). The interaction of both factors ($F(2,38) = 28.76$, $p = 0.048$, $\eta^2 = 0.602$) followed up by post-hoc t-tests revealed that Az after 1-s and 2-s delay phase duration did not differ by temporal expectation (1 s: $t(19) = -1.19$, $p = 0.248$, $r = 0.263$; 2 s: $t(19) = -0.64$, $p = 0.528$, $r = 0.145$). However, after a 4-s delay phase duration, participants performed significantly worse when onset times had been jittered compared to fixed onset times ($t(19) = 2.24$, $p = 0.037$, $r = 0.457$). In addition, we performed single-subject linear fits on fixed and jittered memory decline over time. In line with the findings of Experiment 1, the comparison of the single-subject slopes for fixed and jittered onset times revealed that short-term memory performance (as indicated Az) after jittered onset times decayed faster than after fixed onset times ($t(19) = 2.51$, $p = 0.0213$, $r = 0.499$; see Figure 1D; see Figure 1E for single-subject linear fits. Note that the x-axis has been log-transformed and linear fits thus appear inflected.).

Experiment 2: Effects of memory decay and temporal expectation on alpha power

We were interested in how memory decay was affected by temporal expectation, and how this relationship would relate to alpha-power modulation. Figure 2A (upper panel) illustrates overall power for all frequency bands (5–20 Hz) time-locked to the onset of S1 (averaged across all channels). Figure 2B presents the time-course of alpha power averaged across trials for each condition separately. Following S1, alpha power increases until the earliest occurrence of S2 (i.e., shortest delay phase of 1 second) and then decreases slowly. Inter-trial phase coherence (ITPC; Figure 2A, lower panel) is increased time-locked to the visual cue and the auditory events. Apart from the cue-related response, the ITPC peak frequency is below the alpha range for sound-related responses. In what follows, we will focus on alpha power.

We investigated alpha-power changes as a function of delay phase (–0.8 to –0.1 s time-locked to S2, compare Figure 1) and whether the relationship between delay-phase duration and alpha power was modulated by temporal expectation.

The first-level b-coefficients resulting from the linear regression of alpha power on delay-phase duration were tested against zero on the group level. B-coefficients were significantly smaller than zero in a broad posterior, negative cluster ($p < 0.0001$; see Figure 3A, upper panel) indicating that alpha-power decreased with longer delay-phase duration. A second cluster test contrasting the b-coefficients of the fixed onset-time condition with the b-coefficients of the jittered onset-time condition showed that temporal expectation also had an impact on alpha power: alpha power decreased less with increasing delay-phase durations following fixed onset times compared to jittered onset times (left-posterior positive cluster, $p = 0.025$; see Figure 3B, upper panel).

Source localization of alpha power modulations

Source localizations were computed to identify the brain regions underlying the reported alpha-power effects on the sensor level. The effect of delay-phase duration on alpha power localized to occipital and temporal sites. The negative peak indicating a decrease of alpha power with increasing delay-phase duration emerged from left primary visual cortex (V1, [MNI: –5, –88, 11]). In addition to the negative cluster (retrieved from sensor level analysis), source localization reveals a positive linear relationship between alpha power and delay-phase duration emerging from left STG ([MNI: –50, –17, –8]). Z-transformed effects in source space and z-values greater than 1.96 for each delay-phase condition averaged across vertices around the peak effect in left V1 and left STG are illustrated in line graphs of Figure 3A (lower panel).

The differential effect of temporal expectation on alpha power during the delay phase originated most prominently from left supramarginal gyrus (SMG, [MNI: –54, –37, 32]) and right V1 ([MNI: 14, –80, 13]) (3B, lower panel). In these brain regions, alpha power was higher with longer delays when temporal expectation was present.

Alpha power predicts behavioral performance

In a final analysis, we aimed to relate the observed modulation of memory performance (i.e., Az) to alpha-power modulations. We correlated Az with alpha power, across all conditions, by means of a cluster test, which revealed a centrally distributed positive cluster ($p = 0.022$; Figure 4A). Figure 4B illustrates the source projections of the correlation effect and Figure 4C displays the single-subject correlations between Az and source alpha drawn from left ACC. During the delay phase, the positive correlation of alpha power and Az emerged from left anterior cingulate ([MNI: –2, 2, 38]), bilateral postcentral gyrus ([MNI: 28, –34, 70; MNI: –4, –9, 56]), and bilateral occipital cortices ([MNI: 7, –64, 62; MNI: –7, –86, 2]). A negative correlation between alpha power and Az emerged from left STG ([MNI: –55, –10, –37]).

Note that the positive (V1) as well as negative (STG) correlations of alpha power and performance in this particular analysis are most likely due to the common, confounding variable of delay-phase duration itself, as these regions were identified before to correlate negatively and positively with delay phase duration, respectively.

Figure 4C displays the linear relation of alpha power in left ACC and single-subject, in short-term memory performance accuracy (Az).

Functional connectivity with left STG

Source projections of alpha power revealed a pattern of brain regions susceptible to memory decay. Most prominent effects originated from left STG and bilateral visual cortices. To attain a better understanding of the functional role of alpha power and its different origins, we computed functional connectivity in the alpha range. Due to the strong alpha power effect in left STG (see Figure 3A) as well as its crucial role in auditory short-term memory (Sabri et al., 2004), left STG was used as a seed in a whole brain connectivity analysis. The aim of this analysis was to find brain regions that were functionally connected with left STG, and where this connectivity was modulated by memory decay and temporal expectation.

Connectivity analyses revealed that, with longer delay-phase duration, phase consistency between left STG and bilateral inferior frontal gyrus (IFG; [left MNI: –32, 3, 14], [right MNI: 52, 32, –9]) as well as left pre-motor cortex ([MNI: –6, –12, 63]) increased. In contrast, left-STG connectivity with left primary visual cortex (V1; [MNI: 26, –100, –10]) and right STG ([MNI: 65, –16, 6]) decreased (Figure 4A). Moreover, some memory-decay-related changes in connectivity were modulated by temporal expectation: In right supramarginal gyrus (SMG; [MNI: 62, –35, 40]) as well as in right hippocampus ([MNI: 15, –37, 9]) connectivity with left STG increased with delay-phase duration after fixed onset times and decreased after jittered onset times (see Figure 4B).

To attain a better understanding of the role of functional wPPC-based connectivity with left STG for memory performance, we tested whether inter-individual differences in connectivity between STG

and right V1, as well as between STG and left IFG (i.e., the areas of the decay main effect, see Figure 4), led to inter-individual differences in memory performance (i.e., Az).

We split the group of participants into high and low connectivity groups (median split) for V1 as well as for IFG. Then, we compared performance, as indexed by Az, between high and low connectivity participants using separate mixed-measures ANOVAs (with delay-phase duration [1, 2, 4 s] as a within-subject factor) for V1 and IFG connectivity. For V1, The ANOVA revealed a significant main effect of delay phase duration ($F(2,32) = 18.44$, $p < 0.0001$, $\eta^2 = 0.535$) and a significant main effect of high vs. low connectivity ($F(1,16) = 5.22$, $p = 0.036$, $\eta^2 = 0.246$; see Figure 5). For IFG, the main effect of high vs. low connectivity as well as all interactions did not turn out to be significant (all $F < 1.39$; see Figure 5). The same analysis on the interaction effect in SMG and hippocampus did not yield any significant relationship between degree of functional connectivity and memory performance (i.e., Az).

In sum, these results demonstrate that overall higher alpha-frequency functional connectivity between STG and V1 is beneficial for short-term memory performance.

Discussion

In two experiments, we investigated how decay in auditory short-term memory interacts with temporal expectation and alpha power. The data demonstrate that memory decay can be partially counteracted by temporal expectation. That is, decay is attenuated when the onset time of to-be-remembered items is fixed (and therefore highly predictable) compared to when the onsets are jittered. Second, we observed a potential trading relation between the power of alpha oscillations generated in visual and auditory regions, such that increases of alpha with delay phase were observed in auditory cortices, while decreases were observed in visual cortices. We also observed attenuation of alpha-power modulations by temporal expectation, paralleling memory performance, in functional networks beyond auditory cortex, namely primary visual cortex, bilateral supramarginal gyrus, and hippocampal regions.

Behavioral modelling of memory decay reveals benefit from temporal expectation

In both studies, we were able to replicate the well-established finding that the longer an item is stored in short-term memory, the poorer is memory performance (e.g., Posner and Keele, 1967; Cowan et al., 1997). This can be explained by a “fading away” of the memory representation over time (Brown, 1958).

Critically, both experiments show that the decline of memory performance over time (decay) can be counteracted by temporal expectation. Performance was better when the onset time of the to-be-remembered sound was perfectly predictable compared to when it was jittered. Using an exponential decay function to model behavioral performance (Experiment 1) revealed that the growth factor was

591 increased. We argue here that this factor reflects allocated cognitive resources that counteract the
592 fading away of the memory representation (i.e., decay).
593 Previous work suggests that prior knowledge about the time-of-occurrence of the to-be-
594 remembered item enhances encoding precision during stimulus presentation (Rohenkohl et al., 2012),
595 which in turn enables the maintenance of the item in memory for a longer period. Another (not
596 mutually exclusive) framework, the Time-Based Resource-Sharing model (TBRS; Barrouillet et al.,
597 2004, 2007; Barrouillet and Camos, 2012), suggests that a memory trace requires attention to be
598 maintained, and that the trace decays over time as the attentional focus moves away from the
599 representation. The higher the memory load, the fewer attentional resources are available for memory
600 maintenance (Ma et al., 2014). These interpretations cannot be distinguished based on the analyses
601 performed here. However, we would like to suggest a hybrid model, whereby enhanced encoding
602 precision (due to temporal expectation) frees attentional resources by reducing memory load (Wilsch
603 et al., 2015) and consequently facilitates stimulus maintenance over time.
604
605 **Differential alpha modulations beyond auditory cortex underlie short-term memory and its**
606 **decay**
607 Alpha power during retention was modulated parametrically by delay-phase duration. In line with a
608 decline in memory performance, alpha power decreased over time in bilateral primary visual cortex.
609 Alpha-power decreases during memory delay phases have been reported to emerge from occipito-
610 parietal brain regions (Krause, 1996; Jensen et al., 2002; Jokisch and Jensen, 2007; Tuladhar et al.,
611 2007; Sauseng et al., 2009; Haegens et al., 2010; Bonnefond and Jensen, 2012; Wöstmann et al.,
612 2015). Classically, occipito-parietal alpha power during auditory memory tasks is interpreted as
613 reflecting inhibition of visual areas so that resources can be allocated to maintenance of auditory
614 information.
615 In contrast, in left temporal cortex (i.e., STG encompassing primary auditory cortex), alpha power
616 increased with longer memory-delay times. Based on previous fMRI studies, STG supports active
617 stimulus maintenance during auditory short-term memory (Sabri et al., 2004; Grimault et al., 2009;
618 Kumar et al., 2016). In general, activity in sensory cortices is associated with the maintenance of
619 memory representations (for review on visual short-term memory, see Sreenivasan et al., 2014; for
620 auditory cortex activity, see Linke and Cusack, 2015).
621 Alpha power has been argued to *protect* this storage of items in memory (Roux and Uhlhaas,
622 2014). Corroborating this view, an auditory-memory retroactive-cueing paradigm recently
623 demonstrated increased alpha power in a network including STG after presentation of a retro cue that
624 allowed the participant to select an object from memory and prioritize it (Lim et al., 2015). Thus, we
625 tentatively suggest that the observed alpha-power increase reflects the allocation of attentional
626 resources needed to prevent the fading away of the memory representation over time, rather than
627 inhibitory mechanisms as are classically associated with occipito-parietal alpha. Taken together, the

dissociation between alpha's behavior in visual and auditory cortices supports the presence of distributed alpha systems in the brain, supporting at least partly different functions (Başar et al., 1997).

Finally, with increasing delay-phase duration, the alpha-band functional connectivity between left STG and left IFG as well as between left STG and left pre-motor cortex increased, while such connectivity between the left STG and contralateral right V1 as well as between left STG and contralateral right STG decreased. With respect to the former finding, IFG and pre-motor cortex have both been assigned storage roles in auditory short-term memory (Koelsch et al., 2009). IFG has been shown to be actively involved in phonological maintenance (Paulesu et al., 1993; Awh et al., 1996; Kumar et al., 2016), and specifically so when auditory information cannot be rehearsed, as for tonal stimuli (Gruber and Von Cramon, 2003) or in the present setup.

Notably, Kumar et al. (2016) also observed increased functional connectivity between auditory cortex and left IFG during the maintenance of single tones in memory. They argue that this connectivity is part of a system of auditory short-term memory maintaining sound-specific representations by projections from higher-order areas, such as rehearsal of pitch (Koelsch et al., 2009). Thus, the presently observed increased connectivity between STG on the one hand and IFG and pre-motor cortex on the other would reflect alpha-tuned, active top-down modulations of STG.

In contrast, the decreased connectivity between left STG and left V1 goes well with the overall decrease of alpha power in V1 with longer delay-phase durations. If this decline in alpha power does indeed reflect a decline in functional inhibition, as argued above (see also e.g., Jensen et al., 2002), we suggest that due to this decline in connectivity, irrelevant information emerging from visual cortex is less inhibited and more likely to interfere with the memory representation held active in STG. Not least, we see a functional relevance of this connectivity for optimal memory maintenance: Across participants, overall higher connectivity between STG and V1 was associated with better memory performance (Figure 5).

The benefit from temporal expectation emerges from heteromodal brain areas

One primary goal of the experiments presented here was to determine whether temporal expectation influences memory decay and the accompanying alpha power modulations. In fact, in left supramarginal gyrus (SMG) and in V1, alpha power declined faster following jittered compared to fixed onset times (i.e., behaved similar to memory performance). V1 alpha power arguably inhibits irrelevant information such as interfering visual input. However, the alpha-power decline there is less strong after fixed onset times; possibly indicating enhanced inhibition of irrelevant, visual processing over time.

The SMG has previously been observed to be crucial for stimulus maintenance in auditory short-term memory (van Dijk et al., 2010; Obleser et al., 2012 for increased alpha power in SMG during auditory short-term memory; Paulesu et al., 1993). For example, Lim et al. (2015) found alpha power in SMG to be increased after a valid attention-guiding retro-cue compared to a neutral cue while maintaining a syllable in auditory short-term memory. In their study as well as in the present study,

alpha power was increased when memory maintenance was facilitated due to an attentional cue. Furthermore, Gaab et al. (2003) investigated pitch memory with fMRI and identified bilateral SMG to be a short-term pitch-information storage site. Notably, the BOLD signal emerging from the left SMG correlated positively with performance at the pitch-memory task, underlining the active role of left SMG for auditory short-term memory.

We also observed differential effects of fixed versus jittered sound onsets on alpha connectivity from left STG to right SMG and right hippocampus. Increased connectivity under high temporal expectation further demonstrates the crucial role of SMG for active stimulus maintenance. Hippocampus, considered a vital part of long-term memory (e.g., Jeneson and Squire, 2012), has been found also to play a crucial role in short-term memory maintenance (Graham et al., 2010; Kumar et al., 2016). Underlining the importance of hippocampus for auditory short-term memory, Kumar et al., (2016) demonstrated increased connectivity of right hippocampus and auditory cortex during auditory short-term memory maintenance in particular. Thus, the increase in alpha connectivity of left STG with both areas, SMG and hippocampus, most likely reflects increased neural resource allocation that prevents memory representations from fading away.

Lastly, we tested with a brain-wide analysis for correlations of alpha power and short-term memory performance. A positive correlation in anterior cingulate cortex replicated previous findings that increased alpha power is beneficial for short-term memory or short-term memory performance (Haegens et al., 2010; Roux et al., 2012; Lim et al., 2015; Wilsch et al., 2015). The anterior cingulate cortex, part of the cingulo-opercular network, is crucial for top-down control (for review, see Dosenbach et al., 2007, 2008; Petersen and Posner, 2012). By this view, alpha power provides a task-beneficial ‘steering rhythm’ in and across the relevant top-down attention and sensory networks (e.g., Pinal et al., 2015).

Implications of alpha power for auditory short-term memory

Overall, the present data demonstrate how alpha power serves as a proxy for the degree of decay in short-term memory. However, the brain region in which alpha modulations are observed, as well as the direction of alpha-power changes, informs us regarding the role of alpha oscillations generated in different neural networks. Aligning our alpha-power findings with our modelling analysis of memory performance, we tentatively suggest that increased temporal alpha power after temporally expected stimuli reflects the allocation of additional resources that refresh the representation maintained in memory (Lim et al., 2015; Wilsch and Obleser, 2016). The present data show that the mechanisms by which alpha power impacts on behavioral outcomes are complex and are hardly captured by a singular mechanism, such as functional inhibition. All findings shown here, however, are compatible with a view of alpha-power as a modulatory, top-down signal (Kayser et al., 2015; Sedley et al., 2016; Wöstmann et al., 2017) that can help structure neural signaling. The present findings altogether encourage a more specific perspective on alpha power and its inhibitory role across brain areas and

703 (trial) time. Most importantly, we could demonstrate that temporal expectation can alleviate memory
704 decay, as reflected in memory performance and concomitant alpha power modulations.

705 **References**

706 Awh E, Jonides J, Smith E, Schumacher E, Koeppe RA, Katz S (1996) Dissociation of storage and
707 rehearsal in verbal working memory: Evidence from positron emission tomography. Psychol Sci
708 7:25–31.
709 Bachem A (1954) Time factors in relative and absolute pitch determination. J Acoust Soc Am 26:751–
710 753.
711 Baddeley A (2012) Working memory: theories, models, and controversies. Annu Rev Psychol 63:1–
712 29.
713 Barrouillet P, Bernardin S, Camos V (2004) Time constraints and resource sharing in adults' working
714 memory spans. J Exp Psychol Gen 133:83–100.
715 Barrouillet P, Bernardin S, Portrat S, Vergauwe E, Camos V (2007) Time and cognitive load in
716 working memory. J Exp Psychol Learn Mem Cogn 33:570–585.
717 Barrouillet P, Camos V (2012) As Time Goes By: Temporal Constraints in Working Memory. Curr
718 Dir Psychol Sci 21:413–419.
719 Başar E, Schürmann M, Başar-Eroglu C, Karakas S (1997) Alpha oscillations in brain functioning: an
720 integrative theory. Int J Psychophysiol 26:5–29.
721 Bonnefond M, Jensen O (2012) Alpha oscillations serve to protect working memory maintenance
722 against anticipated distracters. Curr Biol 22:1969–1974.
723 Brown J (1958) Some tests of the decay theory of immediate memory. Q J Exp Psychol 10:12–21.
724 Bull AR, Cuddy LL (1972) Recognition memory for pitch of fixed and roving stimulus tones. Percept
725 Psychophys 11:105–109.
726 Busch NA, Herrmann CS (2003) Object-load and feature-load modulate EEG in a short-term memory
727 task. Neuroreport 14:1721–1724.
728 Coull JT, Nobre AC (1998) Where and when to pay attention: The neural Systems for Directing
729 Attention to Spatial Locations and to Time Intervals as Revealed by Both PET and fMRI. J
730 Neurosci 18:7426–7435.
731 Cowan N (1984) On short and long auditory stores. Psychol Bull 96:341–370.
732 Cowan N, Saults JS, Nugent LD (1997) The role of absolute and relative amounts of time in forgetting
733 within immediate memory: The case of tone-pitch comparisons. Psychon Bull Rev 4:393–397.
734 Cravo AM, Rohenkohl G, Wyart V, Nobre AC (2013) Temporal expectation enhances contrast
735 sensitivity by phase entrainment of low-frequency oscillations in visual cortex. J Neurosci
736 33:4002–4010.
737 Dosenbach NUF, Fair DA, Cohen AL, Schlaggar BL, Petersen SE (2008) A dual-networks
738 architecture of top-down control. Trends Cogn Sci 12:99–105.
739 Dosenbach NUF, Fair DA, Miezin FM, Cohen AL, Wenger KK, Dosenbach RAT, Fox MD, Snyder
740 AZ, Vincent JL, Raichle ME, Schlaggar BL, Petersen SE (2007) Distinct brain networks for
741 adaptive and stable task control in humans. Proc Natl Acad Sci U S A 104:11073–11078.

742 Fuster JM (1999) Memory in the cerebral cortex: An empirical approach to neural networks in the
743 human and nonhuman primate. MIT press.
744 Gaab N, Gaser C, Zaehle T, Jancke L, Schlaug G (2003) Functional anatomy of pitch memory—an
745 fMRI study with sparse temporal sampling. Neuroimage 19:1417–1426.
746 Glass L, Mackey M (1988) From clocks to chaos: the rhythms of life. Princeton University Press.
747 Graham KS, Barense MD, Lee ACH (2010) Going beyond LTM in the MTL: A synthesis of
748 neuropsychological and neuroimaging findings on the role of the medial temporal lobe in
749 memory and perception. Neuropsychologia 48:831–853.
750 Griffin IC, Miniussi C, Nobre AC (2001) Orienting attention in time. Front Biosci 6:d660-671.
751 Grimault S, Lefebvre C, Vachon F, Peretz I, Zatorre R, Robitaille N, Jolicœur P (2009) Load-
752 dependent brain activity related to acoustic short-term memory for pitch:
753 Magnetoencephalography and fMRI. Neurosci Music III Disord Plast Ann New York Acad Sci
754 1169:273–277.
755 Gross J, Kujala J, Hämäläinen M, Timmermann L, Schnitzler A, Salmelin R (2001) Dynamic imaging
756 of coherent sources: Studying neural interactions in the human brain. Proc Natl Acad Sci U S A
757 98:694–699.
758 Gruber O, Von Cramon DY (2003) The functional neuroanatomy of human working memory
759 revisited: Evidence from 3-T fMRI studies using classical domain-specific interference tasks.
760 Neuroimage 19:797–809.
761 Gulbinaite R, İlhan B, VanRullen R (2017) The Triple-Flash Illusion Reveals a Driving Role of
762 Alpha-Band Reverberations in Visual Perception. J Neurosci 37:7219–7230.
763 Haegens S, Osipova D, Oostenveld R, Jensen O (2010) Somatosensory working memory performance
764 in humans depends on both engagement and disengagement of regions in a distributed network.
765 Hum Brain Mapp 31:26–35.
766 Hämäläinen M, Hari R, Ilmoniemi RJ, Knuutila J, Lounasmaa O (1993) Magnetoencephalography-
767 theory, instrumentation, and applications to noninvasive studies of the working human brain. Rev
768 Mod Phys 65:413–497.
769 Han X, Jovicich J, Salat D, van der Kouwe A, Quinn B, Czanner S, Busa E, Pacheco J, Albert M,
770 Killiany R, Maguire P, Rosas D, Makris N, Dale A, Dickerson B, Fischl B (2006) Reliability of
771 MRI-derived measurements of human cerebral cortical thickness: The effects of field strength,
772 scanner upgrade and manufacturer. Neuroimage 32:180–194.
773 Harris JD (1952) The decline of pitch discrimination with time. J Exp Psychol:3–6.
774 Jaramillo S, Zador AM (2011) The auditory cortex mediates the perceptual effects of acoustic
775 temporal expectation. Nat Neurosci 14:246–251.
776 Jeneson A, Squire LR (2012) Working memory, long-term memory, and medial temporal lobe
777 function. Learn Mem 19:15–25.
778 Jensen O, Gelfand J, Kounios J, Lisman JE (2002) Oscillations in the alpha band (9–12 Hz) increase

779 with memory load during retention in a short-term memory task. Cereb Cortex 12:877–882.
780 Jensen O, Mazaheri A (2010) Shaping Functional Architecture by Oscillatory Alpha Activity: Gating
781 by Inhibition. Front Hum Neurosci 4:1–8.
782 Jha AP, McCarthy G (2000) The influence of memory load upon delay-interval activity in a working-
783 memory task: an event-related functional MRI study. J Cogn Neurosci 12:90–105.
784 Jokisch D, Jensen O (2007) Modulation of gamma and alpha activity during a working memory task
785 engaging the dorsal or ventral stream. J Neurosci 27:3244–3251.
786 Joseph S, Teki S, Kumar S, Husain M, Griffiths TD (2016) Resource allocation models of auditory
787 working memory. Brain Res 1640:183–192.
788 Kayser C, Wilson C, Safaai XH, Sakata S, Panzeri S (2015) Rhythmic auditory cortex activity at
789 multiple timescales shapes stimulus–response gain and background firing. J Neurosci 35:7750–
790 7762.
791 Keller TA, Cowan N, Saults JS (1995) Can auditory memory for tone pitch be rehearsed? J Exp
792 Psychol Learn Mem Cogn 21:635–645.
793 Klimesch W, Sauseng P, Hanslmayr S (2007) EEG alpha oscillations: the inhibition-timing
794 hypothesis. Brain Res Rev 53:63–88.
795 Koelsch S, Schulze K, Sammler D, Fritz T, Müller K, Gruber O (2009) Functional architecture of
796 verbal and tonal working memory: An fMRI study. Hum Brain Mapp 30:859–873.
797 Krause CM (1996) Event-related. EEG desynchronization and synchronization during an auditory
798 memory task. Electroencephalogr Clin Neurophysiol 98:319–326.
799 Kumar S, Joseph S, Gander PE, Barascud N, Halpern AR, Griffiths TD (2016) A Brain System for
800 Auditory Working Memory. J Neurosci 36:4492–4505.
801 Kunert R, Jongman SR (2017) Entrainment to an Auditory Signal : Is Attention Involved? J Exp
802 Psychol Gen 146:77–88.
803 Lachaux J-P, Rodriguez E, Martinerie J, Varela FJ (1999) Measuring phase synchrony in brain signals.
804 Hum Brain Mapp 8:194–208.
805 Leiberg S, Lutzenberger W, Kaiser J (2006) Effects of memory load on cortical oscillatory activity
806 during auditory pattern working memory. Brain Res 1120:131–140.
807 Lim S-J, Wöstmann M, Obleser J (2015) Selective attention to auditory memory neurally enhances
808 perceptual precision. J Neurosci 35:16094–16104.
809 Linke AC, Cusack R (2015) Flexible Information Coding in Human Auditory Cortex during
810 Perception, Imagery, and STM of Complex Sounds. J Cogn Neurosci 26:1322–1333.
811 Luck SJ, Vogel EK (1997) The capacity of visual working memory for features and conjunctions.
812 Nature 390:279–281.
813 Ma WJ, Husain M, Bays PM (2014) Changing concepts of working memory. Nat Neurosci 17:347–
814 356.
815 Macmillan NA, Creelman CD (2004) Detection theory: A user's guide, 2nd ed. Mahwah, New Jersey:

816 Lawrence Erlbarun Associates, Inc.
817 Maris E, Oostenveld R (2007) Nonparametric statistical testing of EEG- and MEG-data. J Neurosci
818 Methods 164:177–190.
819 Nees MA (2016) Have We forgotten auditory sensory memory? Retention intervals in studies of
820 nonverbal auditory working memory. Front Psychol 7:1–6.
821 Nobre AC (2001) Orienting attention to instants in time. Neuropsychologia 39:1317–1328.
822 Oberauer K, Lewandowsky S (2013) Evidence against decay in verbal working memory. J Exp
823 Psychol Gen 142:380–411.
824 Obleser J, Eisner F (2009) Pre-lexical abstraction of speech in the auditory cortex. Trends Cogn Sci
825 13:14–19.
826 Obleser J, Wöstmann M, Hellbernd N, Wilsch A, Maess B (2012) Adverse listening conditions and
827 memory load drive a common alpha oscillatory network. J Neurosci 32:12376–12383.
828 Oostenveld R, Fries P, Maris E, Schoffelen J-M (2011) FieldTrip: Open source software for advanced
829 analysis of MEG, EEG, and invasive electrophysiological data. Comput Intell Neurosci
830 2011:156869.
831 Paulesu E, Frith C, Frackowiak R (1993) The neural correlates of the verbal component of working
832 memory. Nature 362:342–345.
833 Percival D, Walden A (1993) Spectral analysis for physical applications: multitaper and conventional
834 univariate techniques. Cambridge: University Press.
835 Petersen SE, Posner MI (2012) The attention system of the human brain: 20 years after. Annu Rev
836 Neurosci 35:73–89.
837 Peterson LR, Peterson MJ (1959) Short-term retention of individual verbal items. J Exp Psychol
838 58:193–198.
839 Pichora-Fuller MK, Singh G (2006) Effects of Age on Auditory and Cognitive Processing:
840 Implications for Hearing Aid Fitting and Audiologic Rehabilitation. Trends Amplif 10:29–59.
841 Pinal D, Zurrón M, Díaz F, Sauseng P (2015) Stuck in default mode: inefficient cross-frequency
842 synchronization may lead to age-related short-term memory decline. Neurobiol Aging 36:1611–
843 1618.
844 Posner MI, Keele SW (1967) Decay of visual information from a single letter. Science (80-) 158:137–
845 139.
846 Rohenkohl G, Cravo AM, Wyart V, Nobre AC (2012) Temporal Expectation Improves the Quality of
847 Sensory Information. J Neurosci 32:8424–8428.
848 Rosenthal R, Rubin DB (2003) $r_{equivalent}$: A Simple Effect Size Indicator Robert. Psychol Methods
849 8:492–496.
850 Roux F, Uhlhaas PJ (2014) Working memory and neural oscillations: alpha–gamma versus theta–
851 gamma codes for distinct WM information? Trends Cogn Sci 18:16–25.
852 Roux F, Wibral M, Mohr HM, Singer W, Uhlhaas PJ (2012) Gamma-band activity in human

prefrontal cortex codes for the number of relevant items maintained in working memory. J Neurosci 32:12411–12420.

Rubin D, Wenzel A (1996) One hundred years of forgetting: A quantitative description of retention. Psychol Rev 103:734–760.

Ruhnau P, Herrmann B, Schröger E (2012) Finding the right control: the mismatch negativity under investigation. Clin Neurophysiol 123:507–512.

Sabri M, Kareken DA, Dzemidzic M, Lowe MJ, Melara RD (2004) Neural correlates of auditory sensory memory and automatic change detection. Neuroimage 21:69–74.

Sadaghiani S, Scheeringa R, Lehongre K, Morillon B, Giraud A-L, Kleinschmidt A (2010) Intrinsic connectivity networks, alpha oscillations, and tonic alertness: a simultaneous electroencephalography/functional magnetic resonance imaging study. J Neurosci 30:10243–10250.

Sauseng P, Klimesch W, Heise KF, Gruber WR, Holz E, Karim A a, Glennon M, Gerloff C, Birbaumer N, Hummel FC (2009) Brain oscillatory substrates of visual short-term memory capacity. Curr Biol 19:1846–1852.

Schoffelen J-M, Oostenveld R, Fries P (2008) Imaging the human motor system's beta-band synchronization during isometric contraction. Neuroimage 41:437–447.

Schröger E (2007) Mismatch Negativity. J Psychophysiol 21:138–146.

Schwarz G (1978) Estimating the dimension of a model. Ann Stat 6:461–464.

Sedley W, Gander PE, Kumar S, Kovach CK, Oya H, Kawasaki H, Iii MAH (2016) Neural signatures of perceptual inference. Elife:1–13.

Sohoglu E, Peelle JE, Carlyon RP, Davis MH (2012) Predictive top-down integration of prior knowledge during speech perception. J Neurosci 32:8443–8453.

Sreenivasan KK, Curtis CE, D'Esposito M (2014) Revisiting the role of persistent neural activity during working memory. Trends Cogn Sci 18:82–89.

Strauß A, Wöstmann M, Obleser J (2014) Cortical alpha oscillations as a tool for auditory selective inhibition. Front Hum Neurosci 8:1–7.

Studebaker GA (1985) A "rationalized" arcsine transform. J Speech, Lang Hear Res 28:455–462.

Taulu S, Kajola M, Simola J (2004) Suppression of interference and artifacts by the signal space separation method. Brain Topogr 16:269–275.

Thorne JD, De Vos M, Viola FC, Debener S (2011) Cross-modal phase reset predicts auditory task performance in humans. J Neurosci 31:3853–3861.

Tuladhar AM, ter Huurne N, Schoffelen J-M, Maris E, Oostenveld R, Jensen O (2007) Parieto-occipital sources account for the increase in alpha activity with working memory load. Hum Brain Mapp 28:785–792.

van den Berg R, Shin H, Chou W-C, George R, Ma WJ (2012) Variability in encoding precision accounts for visual short-term memory limitations. Proc Natl Acad Sci U S A 109:8780–8785.

van Dijk H, Nieuwenhuis ILC, Jensen O (2010) Left temporal alpha band activity increases during working memory retention of pitches. Eur J Neurosci 31:1701–1707.

Vinck M, van Wingerden M, Womelsdorf T, Fries P, Pennartz CMA (2010) The pairwise phase consistency: A bias-free measure of rhythmic neuronal synchronization. Neuroimage 51:112–122.

Watson CS, Wroton HW, Kelly WJ, Benbassat CA (1975) Factors in the discrimination of tonal patterns. I. Component frequency, temporal position, and silent intervals. J Acoust Soc Am 57:1175–1185.

Wickelgren WA (1969) Associative strength theory of recognition memory for pitch. J Math Psychol 61:13–61.

Wilsch A, Henry MJ, Herrmann B, Maess B, Obleser J (2015) Alpha Oscillatory Dynamics Index Temporal Expectation Benefits in Working Memory. Cereb Cortex 25:1938–1946.

Wilsch A, Obleser J (2016) What works in auditory working memory? A neural oscillations perspective. Brain Res 1640:193–207.

Wöstmann M, Herrmann B, Wilsch A, Obleser J (2015) Neural Alpha Dynamics in Younger and Older Listeners Reflect Acoustic Challenges and Predictive Benefits. J Neurosci 35:1458–1467.

Wöstmann M, Lim S-J, Obleser J (2017) The human neural alpha response to speech is a proxy of attentional control. Cereb Cortex 27:3307–3317.

Figure 1. **Experimental design and behavioral performance. A. Experimental design.** The upper panel illustrates a "same" trial (S1 and S2 are the same) with a fixed onset time. The lower panel illustrates a "different" trial (S1 and S2 are different) with jittered onset time. The actual durations of the variable delay phases are specified in **B** and **D**. The light gray box indicates the interval of the spectral analyses: –0.8 to –0.1 s time-locked to S2. **B. Memory performance in Experiment 1**. The gray bars illustrate the six variable delay-phase durations from 0.6 s to 7.0 s (i.e., values in each bar). The line graph displays averaged memory performance in Az (dotted lines) and the exponential fit (solid lines), both separately for fixed and jittered onset times; error bars indicate standard error of the mean of Az. The bar graphs show the average values for the estimated parameters "growth" and "decay", as well as the asymptote, separately for fixed and jittered onset times. Error bars display the standard error of the mean. In all graphs, green refers to fixed and magenta to jittered onset times. The asterisk indicates the significant difference between fixed and jittered onset times. **C**. **Single-participant exponential fits**. Every single plot displays the exponential fit of one participant separately for fixed (green) and jittered (magenta) onset times. Dots display the actual performance data Az. **D**. **Memory performance in Experiment 2.** The gray bars illustrate the three variable delay phase durations from 1.0 s to 4.0 s (i.e., values in each bar). The line graph displays averaged memory performance in Az (RAU-transformed; dotted lines) and the linear fit (solid lines), both separately for fixed and jittered onset times; error bars indicate standard error of the mean of Az. The bar graph shows the average values for the estimated slope, separately for fixed and jittered onset times. Error bars display the standard error of the mean. In all graphs, green refers to fixed and magenta to jittered onset times. The asterisk indicates the significant difference between fixed and jittered onset times. **E**. Single-participant linear fits. Every single plot displays the linear fit of one participant separately for fixed (green) and jittered (magenta) onset times. Note that the x-axis has been log-transformed and linear fits thus appear inflected. Dots display the actual performance data Az.

Figure 2. **Time–Frequency grand averages power and phase coherence. A.** Upper panel: Grand-average power 5–20 Hz averaged across all sensors. Gray arrows on top indicate stimulus occurrence times. S1 refers to the to-be-remembered stimulus. S2 refers to the second stimulus. The index indicates the corresponding delay-phase duration in seconds. Lower panel: Grand average of inter-trial phase coherence 5–20 Hz averaged across all sensors. **B.** Alpha power (8–13 Hz) grand-average across channels per delay-phase duration.

Figure 3. **Condition effects in alpha power**. **A. Effect of memory decay (1, 2, 4 s delay phase).** Upper panel: Topographies of the t-values of the linear fit of alpha power on delay-phase duration on the sensor level. Marked channels present the significant cluster. The line graph represents alpha power extracted from the displayed channels. Lower panel: Source projected linear fit of alpha power on delay-phase duration. Z-transformed t-values are displayed with a threshold of $|z| \geq 1.96$. Line graphs display delay-phase activity drawn from and averaged across the vertices presenting peak activity around left STG and left V1. All error bars show within-subject standard error. **B. Impact of temporal expectation on memory decay.** Upper panel: Topographies of the t-values of the impact of onset-time condition on the linear fit of alpha power on delay-phase duration on the sensor level. Marked channels present significant cluster. Line graphs represent alpha power extracted from the displayed channels. Lower panel: Source projected difference between fixed and jittered onset times of the linear fit of alpha power on delay-phase duration. Z-transformed t-values are displayed with a threshold of $|z| \geq 1.96$. Positive z-values indicate that jittered onset times have a steeper slope than fixed onset times. Line graphs display condition-wise activity drawn from and averaged across the vertices presenting peak activity around left SMG and right V1. All error bars display within-subject standard error.

Figure 4. **Correlation of sensitivity in memory performance (Az) and alpha power A. Topography of the correlation of alpha power and Az (t-values).** Black dots display channels that belong to the significant positive cluster. **B. Alpha power emerging from highlighted brain areas correlates with Az.** Positive z-values indicate a positive correlation of Az and alpha power. **C. Relation of Anterior Cingulate (ACC) alpha power to Accuracy.** The gray lines show the single-subject z-transformed raw data of alpha power in left ACC and Az. The black line indicates the grand average correlation. The blue line of the inlet displays the density of the correlation values across all participants.

Figure 5. **Functional connectivity**. **A. Effect of memory decay (1, 2, 4 s delay phase).** Functional connectivity of left STG and highlighted brain areas is modulated by delay phase duration. Z-transformed t-values are displayed with a threshold of $|z| \geq 1.96$. Positive z-values describe an increase of the phase locking value with delay-phase duration; negative z-values indicate a decrease of phase locking with delay-phase duration. Line graphs display the phase locking value between left STG and right V1 and left IFG respectively for each delay-

phase duration. Error bars represent within-subject standard error. **B. Effect of temporal expectation on memory decay.** Differential impact of fixed and jittered onset times on phase locking of left STG and highlighted brain areas along different delay phases. Z-transformed t-values are displayed with a threshold of $|z| \geq 1.96$. Positive z-values indicate that the slope of the correlation of phase locking and delay-phase duration is greater after fixed onset times than after jittered onset times. Negative z-values indicate that this correlation has a greater slope after jittered than after fixed onset times. Line graphs display the phase-locking value between left STG and right SMG and right Hippocampus, respectively for each delay phase duration and each onset time condition (green line displays fixed and red line displays jittered onset times). Error bars represent within-subject standard error. The brain topography in the center illustrates the seed region (i.e., left STG) of the connectivity analysis. **C. Effect of alpha connectivity on memory performance.** Both plots show memory performance for low and high alpha connectivity (wPPC) between left STG and right V1 (left plot) and left IFG (right plot) for each delay-phase duration. Black lines represent performance after high connectivity, gray lines indicate performance after low connectivity. Error bars indicate standard error of the mean.

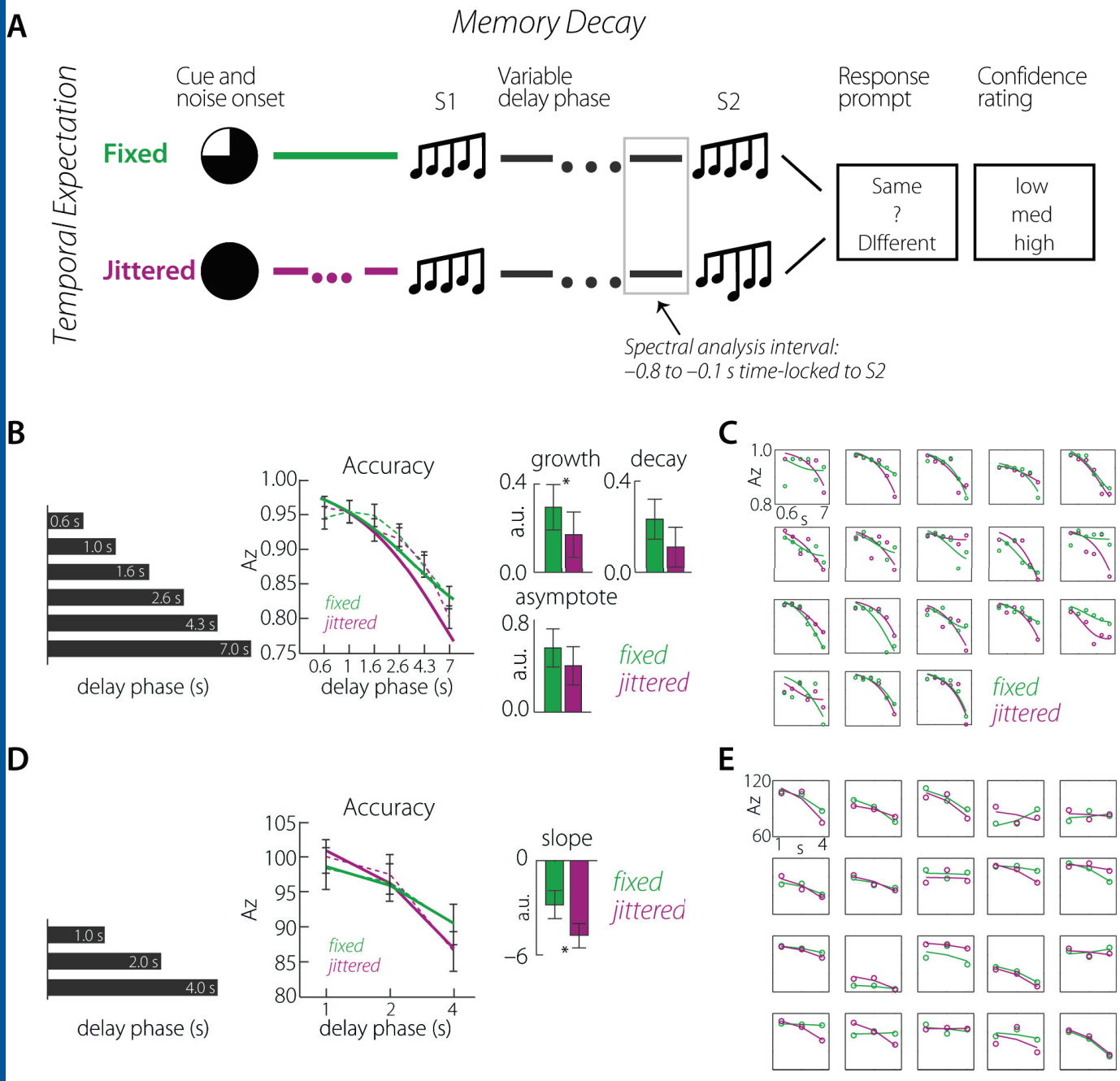

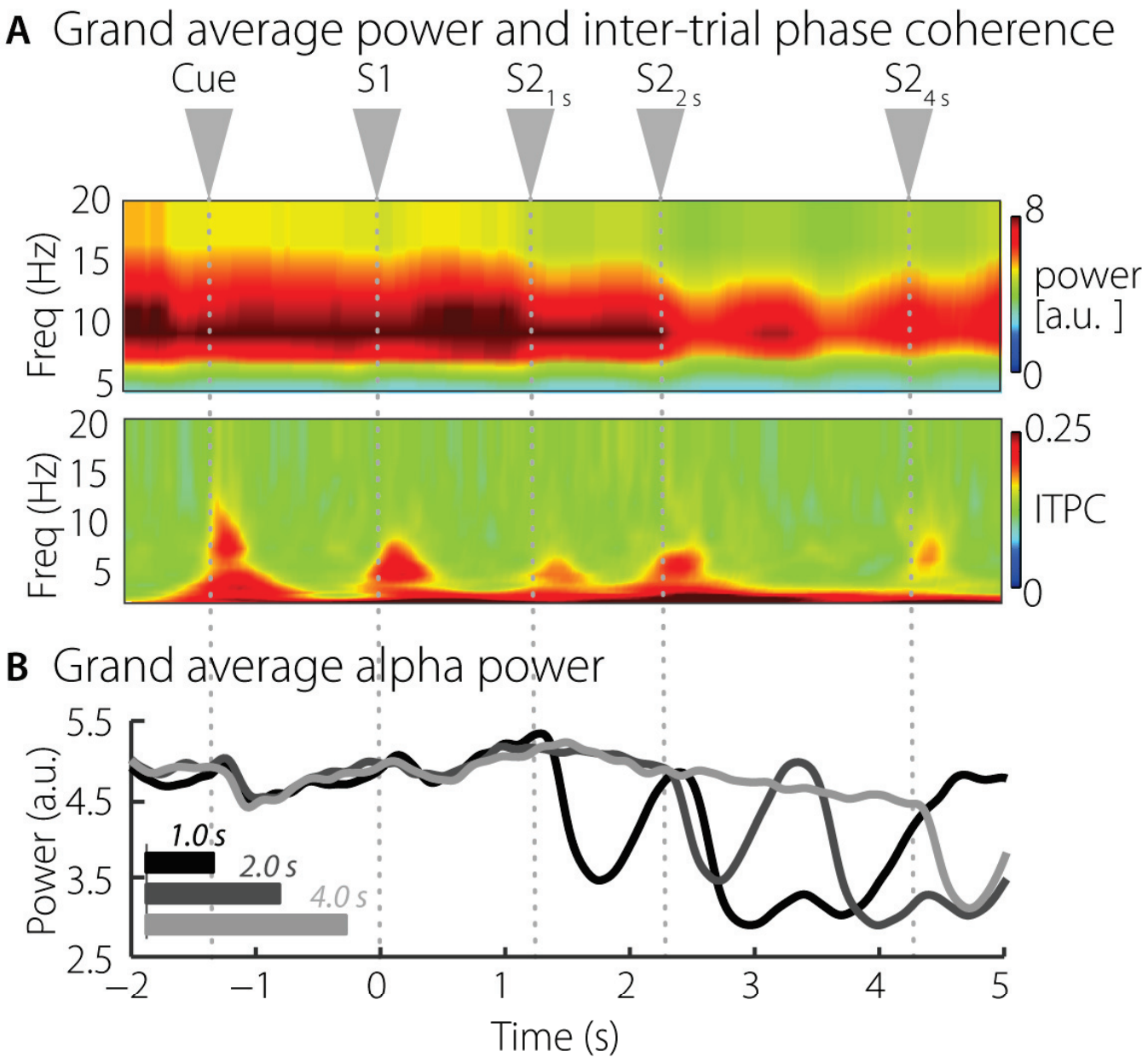

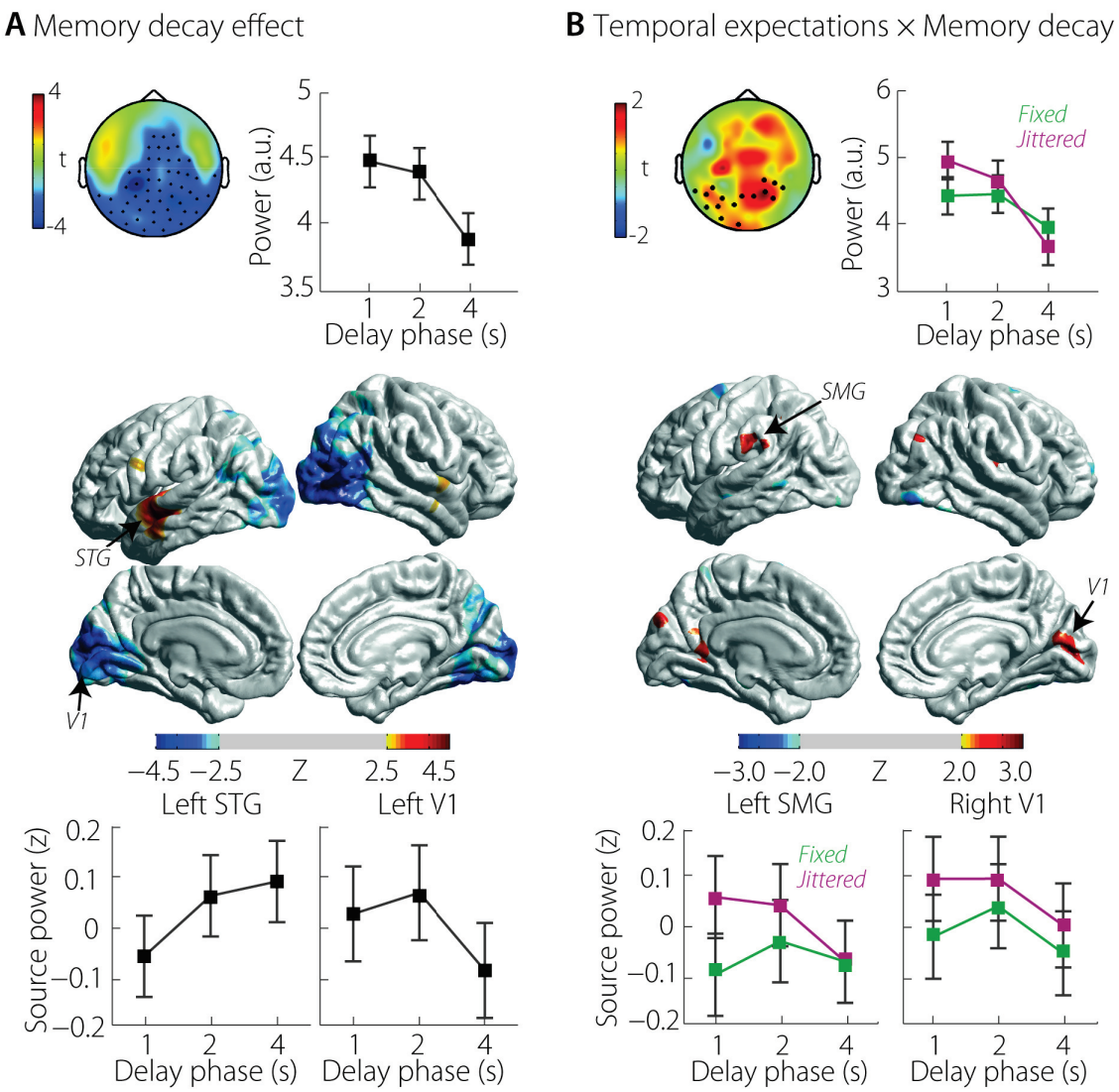

Correlation of Az and alpha power